

RESEARCH

Open Access



Temporally resolved relative krypton neutral density during breathing mode of a hall effect thruster recorded by TALIF

Jacob A. Gottfried¹, Seth Antozzi¹, Jon Stienike¹, Seth J. Thompson¹, John D. Williams¹ and Azer P. Yalin^{1*}

*Correspondence:

Azer P. Yalin
azer.yalin@colostate.edu
¹Department of Mechanical Engineering, Colorado State University, Fort Collins, CO 80523, USA

Abstract

A key issue in the development of theory and models for plasma propulsion devices is to describe the instabilities and fluctuations of the devices. It has been widely recognized that many Hall effect thrusters (HETs) exhibit oscillations at frequencies in the range of ~ 20 kHz. These ionization-related oscillations are generally referred to as Breathing Mode oscillations and have been the subject of considerable research. Here, for the first time, we report direct temporally resolved measurements of the ground state neutral density variation during the period of the oscillation. We used the laser-based Two-Photon Absorption Laser Induced Fluorescence (TALIF) technique to measure neutrals within the plume of a 1.5 kW HET operating on krypton (Kr). Our TALIF scheme employs a frequency-doubled, pulsed dye laser operating at ~ 212 nm to probe ground state Kr atoms. A novel phase-binning approach is used to recover the time-dependent signal by assigning the timing of each collected TALIF signal (laser shot) relative to the phase of the discharge current. We find that the neutral density fluctuates quite strongly over the period of the oscillation, and that this fluctuation leads the current fluctuation as expected.

Keywords Two-photon absorption laser induced fluorescence (TALIF), Hall effect thruster (HET), breathing mode, Temporally resolved, Plasma oscillation, Krypton, Neutral density

Introduction

Electric propulsion (EP) devices operate at significantly higher specific impulse compared to conventional chemical propulsion systems. These devices have been developed and flown for over 50 years, enabling missions with high delta-V requirements. These devices come in many forms, with several performance trade-offs, but today Hall thrusters are the most prevalent EP device used on orbiting spacecraft. The Hall thruster relies on crossed magnetic and electric fields located near the exit of an annular channel to facilitate efficient ionization and acceleration of propellant gases injected into the annulus [1]. The most common propellant gases are the noble gases xenon, krypton, and argon; and the propellant ions are exhausted at velocities of 10's of km/s. A secondary

effect of the highly localized, crossed magnetic and electric fields is large gradients in density, potential, and field strengths that give rise to strong drifts in the plasma that can provide energy to many instabilities and oscillations. Understanding and characterizing these instabilities is required to validate modeling efforts in support of maturing thruster designs and enabling the development of more efficient or higher power Hall thrusters.

One comprehensive review of plasma oscillations found in Hall thrusters was conducted in 2001 by Choueiri [2]. Many of the instabilities and oscillations discussed in the review have been widely studied over the past 20 years and many are still considered open areas of research today. Some of the oscillations have been characterized experimentally and numerically, although there are open questions as to the mechanisms that drive the discharge plasma unstable. One common oscillation in Hall thrusters is referred to as the breathing mode oscillation, which has been widely studied both numerically [3–9] and experimentally [10–16], and despite its identification and early characterization nearly 50 years ago [13], it remains an active area of research. This oscillation is described by strong, coherent, low-frequency fluctuations in the discharge current, typically between ~ 10 – 30 kHz. The breathing mode has been observed to result in longitudinal oscillations in plasma parameters that can be on the order of or greater than the steady-state plasma parameters. Although the general consensus is that the mode is driven by ionization instabilities related to the predator-prey relationship between ionization and neutral particle backfill rate, confirmation of the actual mechanism(s) responsible for the onset of the instability remains an open area of research [7–9].

Furthermore, this oscillation has been observed to exhibit mode shifts, especially in magnetically shielded Hall thrusters operated at lower than nominal power levels [14]. These mode transitions are characterized by larger magnitude current oscillations that pose a risk to on-orbit system stability. Although several models have been developed to predict the conditions and locations where the mode transitions will occur [5, 14], and to describe the propagation of the oscillation from within the channel to areas downstream of the thruster near the exit plane [8], there remains a gap between theoretical modeling efforts and experimental data capable of validating the outstanding physical models.

As Hall thrusters continue to increase in power, the limited pumping capacity of the vacuum test facilities calls into question how the facility impacts the operation of the thruster. These effects have been widely studied experimentally and numerically [17–20], however the understanding of how higher-than-desired facility pressures may impact the stability of the thruster and the plasma oscillations themselves remains an open question [21, 22]. Closing the gap between experimental data of thrusters tested in ground facilities and models of the thrusters will require more capable diagnostics that are able to measure these effects on the time scales relevant to the oscillations of interest.

Dale and Jorns and co-authors have combined time-resolved LIF measurements and electrostatic diagnostic measurements to probe ion and neutral densities and velocity distribution functions (VDFs) inside the Hall thruster channel [8, 14]. While single-photon LIF is well suited for Doppler based velocity measurements, its use for density measurements is more tenuous because one is fundamentally measuring a weakly populated metastable state whose population may not be a reliable representation of the ground state and overall density (because the metastable must be first produced by electron bombardment processes which vary in intensity throughout the channel). Furthermore,

the sensitivity of the diagnostic is limited to regions where the neutral metastable density is sufficiently high, but interference light from the plasma is limited, meaning measurements of the neutral metastable atoms could not be performed with high confidence at axial positions near the ionization region or further downstream within the plume (where excitation is reduced). An important aspect of understanding how the breathing mode instability responds to facility pressure is to understand how the neutral density oscillates through these regions including near the channel exit.

Standard LIF techniques can provide neutral and ion VDFs based on Doppler shifting, but electrostatic probes (i.e. Langmuir and Faraday probes) are often used to measure absolute ion currents in the nearfield and to estimate changes in properties like electron temperature [8, 14, 15]. Although these measurements are useful in providing important plasma parameters for modeling efforts, the extent to which they can be used in the near field and channel is limited due to their perturbative effects [23, 24]. Furthermore, no common electrostatic probe is available to provide neutral particle density fluctuations in the near field without perturbing the natural plasma state. The present work extends our past use of two photon absorption laser induced fluorescence (TALIF) for reliable measurement of neutral populations [25–27] – by probing the ground state – but now for temporally resolved measurements relative to the breathing mode oscillation. The main advantage of TALIF for density measurements is that by using two-photon absorption we can access the relatively large energy gaps between the ground state and excited states, thereby accessing ground state transitions with available tunable laser systems typically operating in the range of $\sim 200\text{--}250$ nm [25–33]. Two general disadvantages of TALIF detection are that signal-to-noise can be poor owing to small two-photon absorption cross-sections (and competing luminosity from the same emission lines) and that data is generally collected with low repetition-rate pulsed lasers ($\sim 10\text{--}20$ Hz). As presented herein, in this work we propose and demonstrate a novel phase-binning method allowing us to synchronize the individual TALIF signals to the thruster discharge current oscillation, from which we can reconstruct the phase- (time-) dependent neutral density variation relative to the current oscillation [34]. Section 2 of the paper summarized the experimental setup and method for the TALIF experimental setup and data-acquisition. Section 3 provides results and discussion of using the method to study the Kr density variation in a 1.5 kW Hall thruster. Finally, conclusions and future work are discussed in Sect. 4.

Experimental setup and methods

The following sections contain details on our experimental setup and data collection and analysis.

Optical layout and thruster setup

This work employs two-photon absorption laser-induced fluorescence (TALIF) using a 212.6 nm excitation scheme with detection at 760 nm following our past Kr TALIF work [26, 27]. The optical setup is shown in Fig. 1. The laser source is a nanosecond pulsed dye laser (Sirah Precision Scan) pumped by the third harmonic (355 nm) output of an Nd:YAG laser (Spectra-Physics Quanta Ray Lab 150–10). Exalite 428 dye is used to produce visible light at 425 nm which is then doubled using an integrated frequency conversion unit. The final output of the laser is a rectangular beam (approx. 2×6 mm) with a

pulse duration of $\sim 9 \pm 1$ ns full-width at half-maximum (FWHM) and a pulse energy of 2.5 mJ. The energy setpoint was chosen as it produces a saturated TALIF response with our delivery optics [27]. Using a periscope, the beam is steered through an ultraviolet (UV) grade fused silica window into the vacuum chamber where it is brought to a weak focus by a plano-convex lens with a focal length of 50 cm. The TALIF signal, along with the plasma's luminous emission, is collected and collimated by a 5 cm diameter, 30 cm focal length plano-convex lens at an angle perpendicular to the probe beam. The collected light is focused onto a multimode optical fiber (Thorlabs M29L02) with a core diameter of 0.6 mm by a 5 cm diameter 15 cm focal length plano-convex lens. The overall imaging train has a magnification factor of 0.5 such that the resulting collection area at the collection location (waist of the 212 nm probe beam) is a circle with a diameter of 1.2 mm. The collection area is roughly an order of magnitude larger than the probe laser waist to increase resilience against micro-movements of the beam delivery and collection optics during chamber evacuation and heating. The collected light is coupled out of the vacuum chamber, via a bulkhead mounted feedthrough, into a second identical fiber optic the output of which is 1-to-1 imaged onto a photomultiplier tube (PMT, Hamamatsu R3896) equipped with a bandpass filter (Thorlabs FBH760-10) to remove most of the plasma emission that originates at other emission lines as opposed to 760 nm.

The Hall Effect thruster used in this work is a 1.5 kW SPT-like thruster with a center mounted 25 A class Ba-O based hollow cathode. The thruster is mounted on a thrust stand within a 1.7 m diameter by 4.6 m long cylindrical vacuum chamber pumped by a Leybold DryVac 650 roughing pump and two 24" Varian diffusion pumps and two cryo sails resulting in roughly 17,000 L/s of pumping speed on Kr. The thruster is positioned near the centerline of the vacuum chamber and approximately 2 m axially from the end as shown in Fig. 1. The base pressure is $\sim 10^{-6}$ Torr measured by a Granville Phillips 390 Micro-Ion vacuum gauge ($\pm 15\%$ accuracy) located approximately 0.5 m behind the thruster on chamber wall.

The thruster is operated on ultra-high purity krypton gas (99.999% pure) at an anode and cathode mass flow rate of 50 and 4 sccm respectively. The mass flow rates are controlled by Alicat Scientific mass flow controllers with manufacturer stated ± 0.1 sccm accuracy. The thruster discharge is operated at a 300 V with a time averaged anode

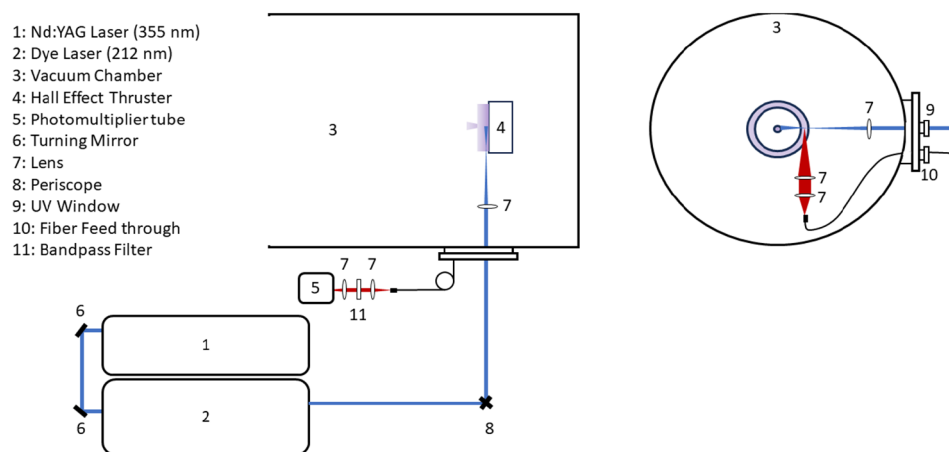


Fig. 1 Setup for TALIF measurements of plasma thruster. Left: External view of chamber. Right: Optics inside vacuum chamber

current of 5 A, the nominal 1.5 kW operating condition of the thruster. However, the thruster was operated with a weaker magnetic field that resulted in strong breathing mode oscillations, with peak-to-peak currents approaching nearly 400% of the nominal steady-state anode current. During operation, the corrected chamber background pressure is 4×10^{-5} Torr. Propellant enters the thruster discharge channel through several orifices spaced evenly on the downstream face of the anode ring in the back of the Borosil channel. The waist of the TALIF probe beam is positioned at the same radial location as the channel outlet orifices and at axial position of several mm downstream of the channel/thruster face.

Data collection

To measure temporally resolved densities relative to the breathing mode oscillations, we reference the individual TALIF signals (from individual laser shots) to the timing of the discharge current fluctuations. In our method, we allow the laser to free-run at its design pulse repetition rate of 10 s^{-1} and record the timing of each TALIF signal (laser shot) relative to the thruster current oscillation. To record both the TALIF signal (PMT output) with sufficient temporal and voltage resolution as well as the thruster current oscillation (breathing mode), two oscilloscopes with separate time bases were used. Both oscilloscopes are triggered simultaneously by a photodiode located within the dye lasers frequency conversion unit. The output of each oscilloscope is logged and saved to a computer with a custom LabView code. The breathing mode current is measured with a current probe (Rigol RP1002C) and recorded with a Rigol DS1054 oscilloscope where the time base is set to a recording length of $120 \mu\text{s}$ with the trigger at the center of the recording. The time base was selected to ensure at least one full period of the breathing mode is captured. The PMT output is recorded with a Tektronix TDS5034B oscilloscope with a recording length of 200 ns. In addition to the PMT signal, the high-speed oscilloscope also records the instantaneous current probe measurement as an additional check to verify both scopes are properly synchronized. A given measurement campaign, to yield the temporal dependence relative to the oscillations, typically comprised the acquisition of $\sim 12,000$ individual laser shots which corresponds to ~ 20 min of experimental time given the laser pulse repetition rate of 10 Hz. The current setup has a latency issue in the data collection such that only 50% of the shots can be acquired meaning that ~ 40 min was required to obtain the aforementioned data.

Data analysis

The experimental TALIF data is binned into $N=20$ equally sized phase-bins based on the timing of the TALIF (laser shot) relative to the phase of the breathing mode, where phase of zero and 2π is defined to coincide with maxima (peaks) of the discharge current fluctuation. As shown in Fig. 2, the phase, ϕ , of a given TALIF signal shot is defined as:

$$\phi(t) = 2\pi * \frac{t-t_0}{T}$$

where T is the (local) breathing mode period (found from spacing of the preceding and following peaks), t_0 is the time of the preceding breathing mode peak, and t is the time of the laser pulse. In cases ($<3\%$) where multiple peaks are not present in the current trace recording, the shot is discarded from the analysis due to insufficient phase classifying

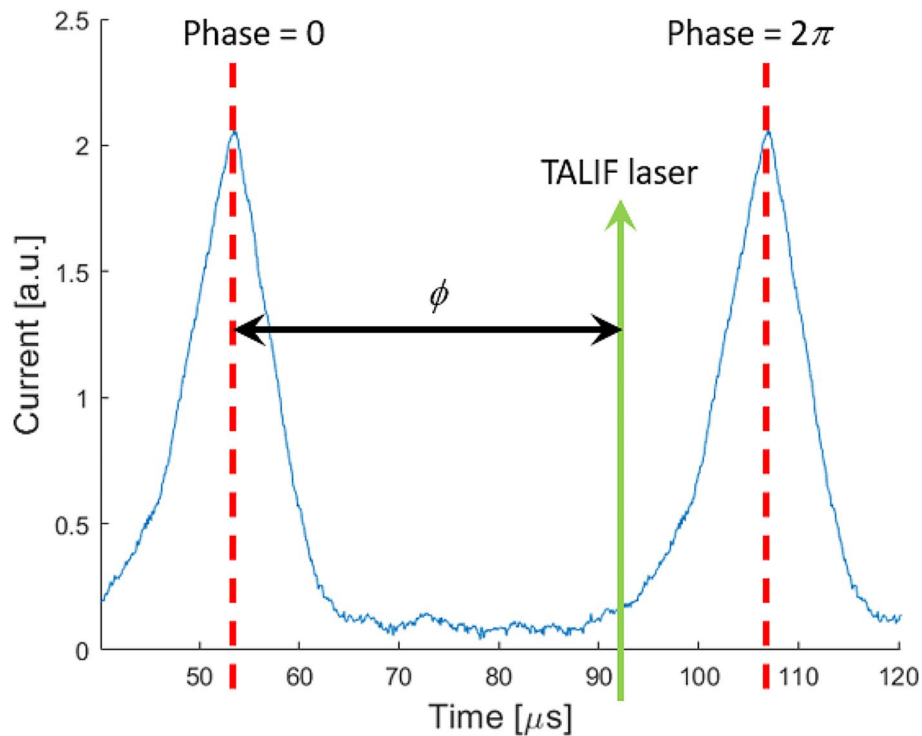


Fig. 2 Approach for determining the phase of an individual TALIF measurement relative to the breathing mode oscillation period

information. In this way, each (qualifying) TALIF measurement is assigned to one of the N phase bins (where each bin has extent $2\pi/N$, starting from $f=0$).

Within each phase bin, the data associated with individual laser shots are arbitrarily sub-divided into groups of $n=100$ individual shots. The groupings of 100 PMT traces are averaged and analyzed to yield a smaller number of final data point for reporting. Averaging of the individual PMT traces is required to improve the signal-to-noise ratio and the reliability of baseline subtraction given the random variance of naturally occurring plasma luminosity at the TALIF collection wavelength as has been discussed in previous work [26]. Each trace is the PMT voltage versus time with the data-acquiring oscilloscope triggered to gather data over 200 ns around the TALIF signal. We first determine a signal baseline based on averaging 50 data points that are earlier in time and 50 points that are later in time, relative to the TALIF signal. As will be discussed below, the baseline is primarily due to plasma luminosity and carries plasma diagnostic information also. The baseline is then subtracted from the averaged PMT trace. After baseline subtraction, the PMT trace is numerically integrated to form the TALIF signal, which is linearly proportional to the neutral Kr number density [26–29]. By examining these TALIF signals versus their assigned phase we can measure neutral density variation across a breathing mode cycle.

Results and discussion

Current oscillation and breathing mode statistics

The left of Fig. 3 shows representative examples of discharge current oscillations as recorded by the current probe and oscilloscope. Three different traces are shown to get a sense of the variations. Each trace is 120 μs in extent (with the TALIF laser fired at

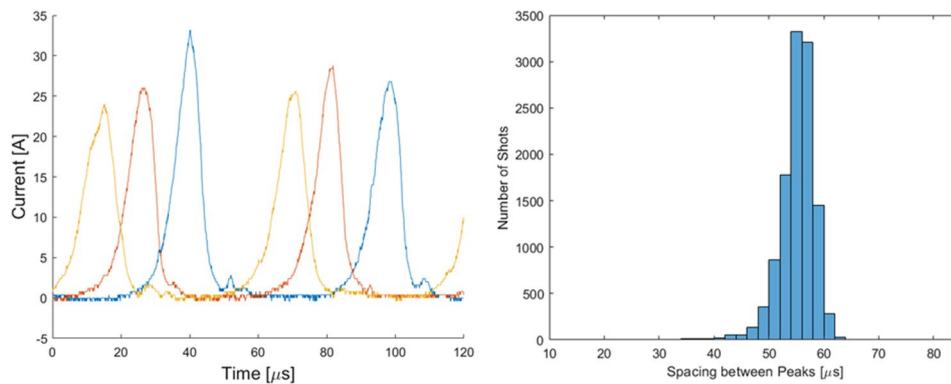


Fig. 3 Left: Example current traces showing breathing mode oscillations (3 different traces shown). Right: Histogram of recorded oscillation periods as given by spacings of consecutive current pulses

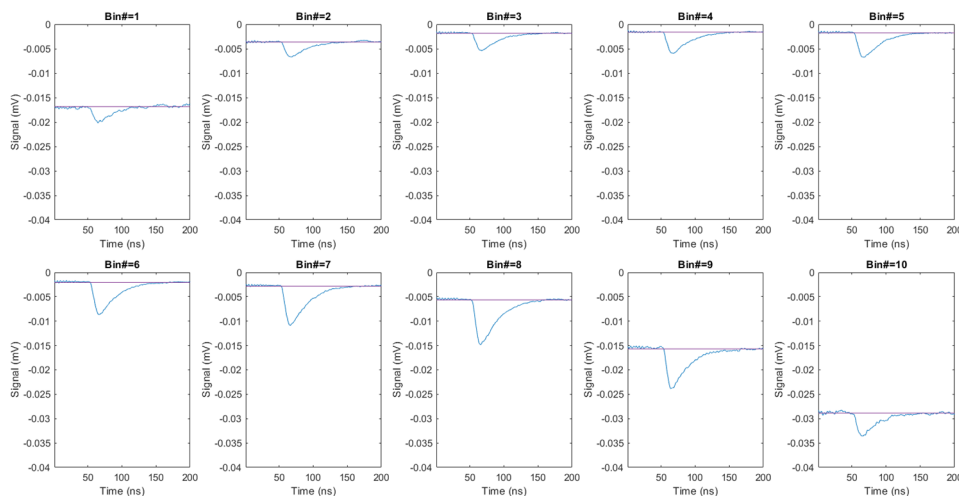


Fig. 4 TALIF signals across 10 phase bins of the oscillation period

exactly the midpoint of each trace). The observed current fluctuations in the thruster under study are rather strong, on the order of 500% in terms of the ratio of peak (~ 25 A) to mean (5 A), and quite periodic. The right of Fig. 3 shows a histogram of the oscillation periods as found from pairs of current peaks from all recorded current traces using the method of Fig. 2. While the observed period has some spread (drift), we find the values to be quite tightly grouped in a single distribution with mean of $55.1 \mu\text{s}$ (~ 18.1 kHz) and standard deviation of $3.26 \mu\text{s}$ where the observed frequency is consistent with past findings of breathing mode oscillations.

Phase-resolved TALIF signals

Using the methods described above, we have binned all collected TALIF signals into uniformly sized phase-bins. Figure 4 shows a case where we have formed $N=10$ phase-bins and each panel shows a single representative PMT waveform trace due to 100 averaged shots belonging to the bin. (Subsequent analysis will use $N=20$ phase bins but we use $N=10$ to have a more manageable figure.) The bins from 1 to 10 span a single period of the oscillation (with current peaks at the start/end of the period). The laser is fired at time of ~ 75 ns (relative to the start of the traces) and the TALIF signal is visible as

a downward waveform (blue curve) relative to the baseline (pink line), given that the PMT provides negative voltages. The areas of these downward waveforms correspond to the Kr density during the corresponding bin such that comparing the panels immediately reveals the basic trends of neutral density variation. Figure 5 shows the phase (bin) resolved TALIF signals, in this case with $N=20$ bins. We plot as the fractional phase (i.e., phase divided by 2π) such that current maxima are at 0 and 1 (spaced by $\sim 55.1 \mu\text{s}$ in time). The plot shows the individual data points (black) found as averages of $n=100$ raw traces (laser shots) along with final data points and error bars for each phase value, found as the mean and standard-deviation, respectively, of the corresponding individual points. The plots shows a clear variation of the TALIF signal (neutral density population) versus phase as is further discussed below.

Reconstructed neutral density variation over the oscillation

Figure 6 shows the reconstructed neutral density (TALIF signal) and current oscillation. We plot the data from a single period over 2.5 periods for visual clarity. The TALIF phase analysis uses 20 bins and the displayed current trace (I_d) is found from averaging 5 randomly selected current measurements. The plotted neutral density data points (blue curve) are shown centered in their temporal bins where we have converted the phase back to time, based on the mean period of $55.1 \mu\text{s}$. To the best of our knowledge, these data represent the first direct observation of the neutral ground state density variation during plasma fluctuations within a HET.

It is interesting to consider the neutral density oscillation in the context of the dynamics of the ionization region, i.e., the breathing mode and the predator-prey interpretation of the ionization-induced oscillation [8, 14, 35, 36]. To this end, we should account for the transit time of neutrals between the ionization region (where the dynamics originate) and the actual TALIF measurement location. The timing of the discharge current is essentially independent of position (due to fast moving electrons); however, neutrals move with speeds that are not negligibly fast. We also plot a time-shifted curve (red), by

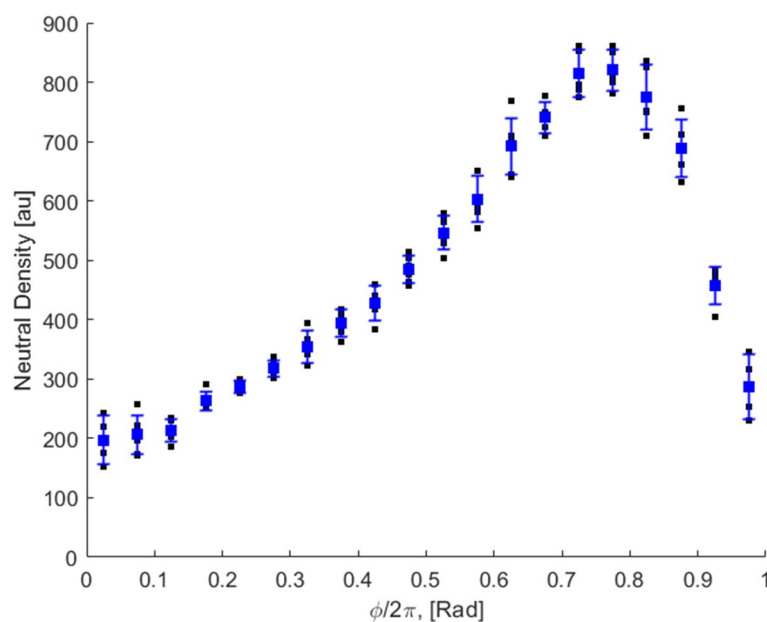


Fig. 5 TALIF signal versus phase angle over one oscillation period (20 phase bins)

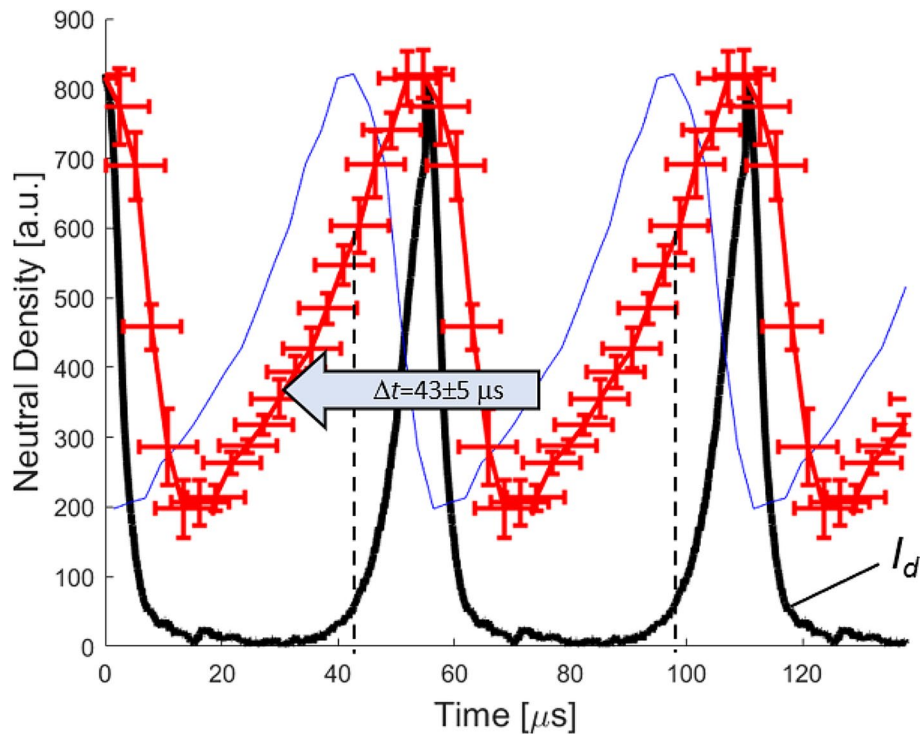


Fig. 6 Time-resolved TALIF measurement of neutral density during period of HET breathing-mode fluctuation (shown over 2.5 periods for visual clarity). Blue trace: Density variation based on phase analysis. Red trace: Same density variation but time-shifted to earlier time by $\Delta t = 43 \pm 5 \mu\text{s}$ to account for time-of-flight between upstream ionization region and the measurement location. Vertical dashed lines show times approximate times of (periodic) current increase

a differential $\Delta t = 43 \pm 5 \mu\text{s}$, toward earlier time. This curve represents the inferred temporal variation of neutrals in the ionization region. The value of the time shift is found as $\Delta t = \Delta L / V$, where V is the mean neutral bulk velocity and ΔL is the separation distance between the measurement location and ionization region. We assume a thermal velocity of $V \sim 370\text{--}390 \text{ m/s}$ (due to anode temperature of $\sim 550\text{--}600 \text{ K}$) and a distance Δ of $L \sim 15\text{--}18 \text{ mm}$ between the measurement location ($\sim 5 \text{ mm}$ downstream of the exit plane) and end of ionization region (expected to be $\sim 1\text{--}1.3 \text{ cm}$ upstream of the exit plane based on magnetic field mapping). The observed dynamics of the time-shifted curve relative to the current appear consistent with our understanding of the breathing mode behavior. We find that the neutral density fluctuation *leads* the current fluctuation, i.e., the rise in neutral density occurs *before* the rise in current. We also see that the rise in current (dashed vertical lines shown as rough guide) occurs along the rising limb of the neutral density increase and that the decrease in neutral density is close, or slightly upstream, to the time of the current maximum, all in agreement with recent literature [14, 36]. This behavior is consistent with the predator-prey interpretation of the breathing mode where the (depleted) neutral density needs to fill the channel to a critical level *after* which ionization rates increase and lead to elevated ionization and a maximum in the discharge current.

In future work we will more precisely determine the spatial distance between the measurement region and ionization region (e.g., by also using probes or LIF of ions to more accurately locate the ionization region). The use of a constant time-shift assumes a static ionization region but several studies have suggested that the ionization region itself

shifts during the oscillation [9, 16, 37]. TALIF data of the type shown here, particularly if recorded at a series of axial locations, can contribute to understanding these phenomena, for example, the velocity and phasing of neutral density waves will be immediately visible by tracking the time of the rising limb of neutral density (as synchronized to the current) at different TALIF axial measurement locations.

Reconstructed TALIF baseline over the oscillation

Our primary interest is to study the TALIF signal due to fluorescence of the neutrals but the detector (PMT) baseline voltage also shows periodic trends versus the fluctuation. In Fig. 4, each panel shows PMT voltage traces for a given phase bin. In each panel, the baseline (pink line) is due to (non-TALIF) plasma luminosity detected by the PMT. (Note that the dark current contribution is negligible on this scale.) Fig. 7 shows a plot of the average baseline values (again found from the data points based on the groupings of $n=100$ raw traces) plotted versus the discharge current oscillation. We observe that the TALIF baseline, which is just optical emission from the plasma recorded through the filters, correlates closely with discharge current. Because the emission derives from excited states of the plasma, it is reasonable that the emission will be closely linked to the current since elevated electron density and temperature generate the plasma excited states. This type of plasma luminosity can be collected quite easily (even with no laser) and there may be some utility in using it as a marker (or check) for discharge current.

Reference cells

The TALIF measurements presented in this contribution are relative measurements (proportional to neutral Kr density). Future work will use a calibration approach based on scaling TALIF signals collected from known-density reference cells (with the same beam delivery and signal collection). The use of reference cells, as opposed to filling the overall chamber to a known gas density, is generally preferred owing to possible spatial

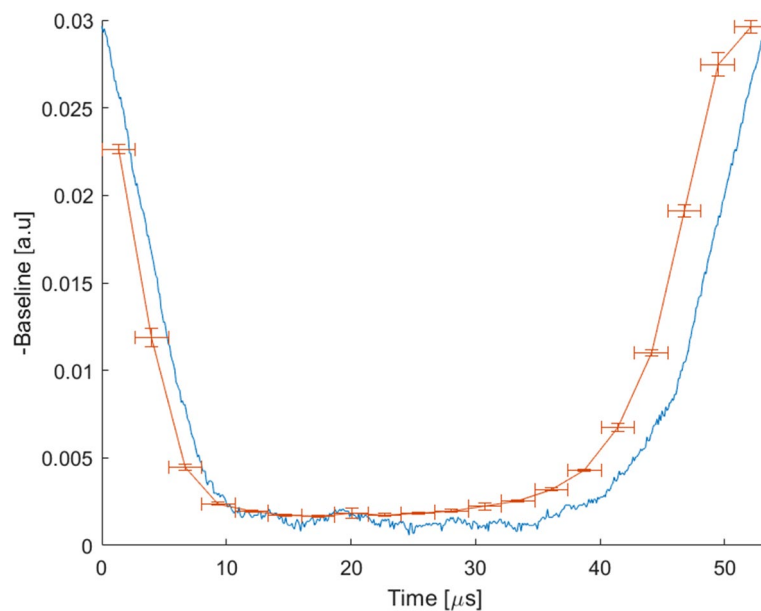


Fig. 7 Time-resolved TALIF baseline (orange) and discharge current (blue) during one period of HET breathing-mode fluctuation

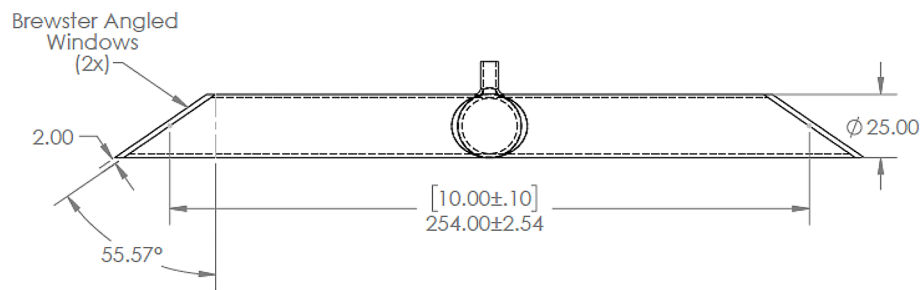


Fig. 8 Schematic diagram of reference cell design. (Dimensions in mm.)

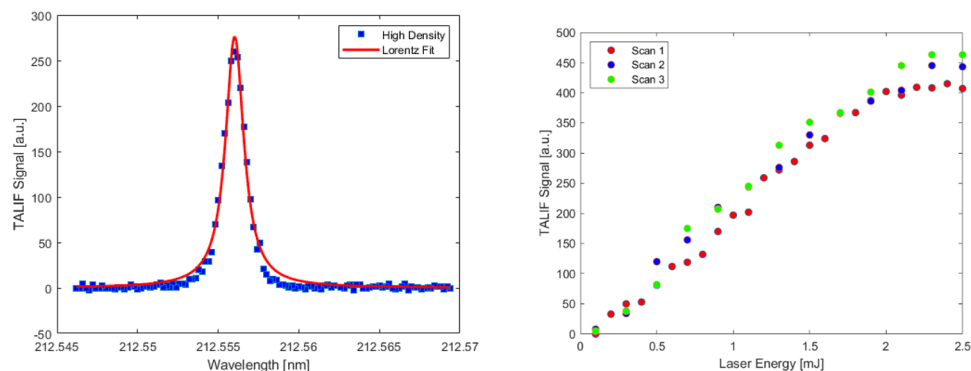


Fig. 9 Left: TALIF wavelength scan of high density cell. Right: Energy dependence study of TALIF signal from high density cell

variations in chamber pressure associated with the detailed flow and pumping configuration. We have two reference cells filled with a gas mixture of Krypton and Argon at two known concentrations. The Ar acts as a buffer gas and makes the overall cell pressure higher and more amenable to practical filling. The molar concentration of Kr within the mix is 1000 ppm. The high-density cell is at 100 mTorr (at room temperature) corresponding to Kr density of $3.24 \times 10^{12} \text{ cm}^{-3}$, while the low-density cell is at 10 mTorr giving a density on the order of $3.24 \times 10^{11} \text{ cm}^{-3}$. As shown in Fig. 8, the cells have Brewster windows to couple the light in and out with minimal spurious reflections, and flat fused-silica windows on the side for collection of TALIF light.

The right of left of Fig. 9 shows a TALIF wavelength scan across the Kr absorption feature clearly showing the resonance. The data was collected using the same beam delivery and light collection as used in the TALIF experiments, and future work will use this approach to quantify measured TALIF signals. We can also use the reference cells for studies of how the TALIF signal depends on laser energy and we can compare those results with our rate-equation modeling [38]. The right of Fig. 9 shows an initial study of TALIF signal versus laser energy. Most of our experiments are performed in the laser energy range of $\sim 1.5\text{-}2$ mJ where the measurements show a nearly linear signal dependence on energy (consistent with the model). The energy dependence shows positive curvature at very low energies, expected due to the quadratic nature of the 2-photon absorption step, and then appear to have some roll-off at the highest energies which may be due to increasing the photoionization loss (with goes roughly as intensity cubed due to the 2+1 ionization process).

Conclusion

We have presented a new and simple method for making temporally (phase-) resolved measurements in plasma thrusters based on data obtained with low repetition-rate pulsed lasers. The method is demonstrated here for TALIF measurements of neutral (Kr) atom density within the plume of a HET. Measurements presented in this work are proportional to neutral Kr density but are relative measurements. Future work will provide absolute Kr densities by scaling against signals from calibrated reference cells. The time-resolved measurements show pronounced density variations over the period of the breathing mode, and the high contrast is likely connected to the quite strong and periodic current fluctuations of the studied thruster. While demonstrated here for Kr, the same scheme should be applicable to TALIF of Xenon also [25, 29, 30]. The scheme presented may be applicable to other oscillations also, as long as they are quite strongly periodic, up to a frequency of ~ 1 MHz based on raw measurements needing ~ 100 ns and requiring a minimum of 10 phase-bins, but this should be demonstrated experimentally.

The approach should afford many avenues for future research in connection with unraveling the complex physics of Hall thruster breathing oscillations. For example, it will be interesting to perform similar measurements at a series of axial positions along the thruster center line. Each measurement will be referenced against the (same) current fluctuation, such that the measurements at different axial locations should directly capture the wave motion of neutrals along the thruster axis. Another line of investigation will be to examine how the breathing mode oscillations, and associated neutral density fluctuations, vary with chamber background pressure, which will be important in connection with understanding the facility effects associated terrestrial testing and differences from in-space operation.

Author contributions

A.Y. conceived the experimental approach. A.Y. and J.W. obtained funding. J.G. led the detailed laser experiments with support from S.A. and J.S. S.T. and J.W. led the operation of the thruster facility. J.G. and A.Y. led the writing of the manuscript with help from S.T. and J.W. All authors reviewed the manuscript.

Funding

This work was supported by NASA through the Joint Advanced Propulsion Institute, a NASA Space Technology Research Institute, grant number 80NSSC21K1118. This work was also supported by the National Science Foundation Division of Physics under Award No. 2010466.

Data availability

No datasets were generated or analysed during the current study.

Declarations

Competing interests

The authors declare no competing interests.

Received: 14 January 2024 / Accepted: 9 April 2024

Published online: 13 May 2024

References

1. Goebel DM, Katz I, Technology Series (2008) Fundamentals of electric propulsion: ion and hall thrusters. JPL space science
2. Choueiri EY (2001) Plasma oscillations in hall thrusters. *Phys Plasmas* 8(4):1411–1426
3. Fife J et al (1997) A numerical study of low-frequency discharge oscillations in hall thrusters. In 33rd joint propulsion conference and exhibit
4. Boeuf JP, Garrigues L (1998) Low frequency oscillations in a stationary plasma thruster. *J Appl Phys* 84(7):3541–3554
5. Hara K et al (2014) Mode transition of a Hall thruster discharge plasma. *J Appl Phys* 115(20)
6. Hara K et al (2014) Perturbation analysis of ionization oscillations in Hall effect thrusters. *Phys Plasmas* 21(12)
7. Chapurin O et al (2021) On the mechanism of ionization oscillations in Hall thrusters. *J Appl Phys* 129(23)
8. Dale ET, Jorns BA (2021) Experimental characterization of Hall thruster breathing mode dynamics. *J Appl Phys* 130(13)

9. Lafleur T, Chabert P, Bourdon A (2021) The origin of the breathing mode in Hall thrusters and its stabilization. *J Appl Phys* 130(5)
10. Sekerak MJ et al (2016) Mode transitions in Hall-effect thrusters induced by variable magnetic field strength. *J Propul Power* 32(4):903–917
11. Huang W, Kamhawi H, Haag T Plasma oscillation characterization of NASA's HERMeS Hall thruster via high speed imaging. In 52nd AIAA/SAE/ASEE joint propulsion conference
12. Jorns B, Hofer RR (2014) Plasma oscillations in a 6-kW magnetically shielded Hall Thruster. *Phys Plasmas*
13. Esipchuck Y et al (1974) Plasma oscillations in closed-drift accelerators with an extended acceleration zone. *Sov Phys Tech Phys* 18(928)
14. Jorns BA et al (2022) Prediction and mitigation of the mode transition in a magnetically shielded hall thruster at high-specific impulse and low power. In 7th International Electric Propulsion Conference. Cambridge, MA
15. Lobbia RB (2010) A time-resolved investigation of the Hall thruster breathing mode. University of Michigan: United States-Michigan. 179
16. Chaplin VH et al (2020) Time-resolved ion velocity measurements in a high-power hall thruster using laser-induced fluorescence with transfer function averaging. *Appl Phys Lett* 116(23)
17. Frieman JD et al (2016) Electrical Facility effects on Hall Thruster Cathode Coupling: performance and Plume properties. *J Propul Power* 32(1):251–264
18. Brown DL, Gallimore AD (2011) Evaluation of Facility effects on Ion Migration in a Hall Thruster Plume. *J Propul Power* 27(3):573–585
19. Randolph T et al (1993) Facility effects on stationary plasma thruster testing. In 23rd international electric propulsion conference. Worthington, OH
20. Jorns BA, Byrne MP (2021) Model for the dependence of cathode voltage in a Hall thruster on facility pressure. *Plasma Sources Sci Technol* 30(1):015012
21. Walker JA et al (2016) Electrical Facility effects on Hall-Effect-Thruster Cathode Coupling: Discharge oscillations and Facility Coupling. *J Propul Power* 32(4):844–855
22. Kamhawi H et al (2016) Performance, facility pressure effects, and stability characterization tests of NASA's Hall effect rocket with magnetic shielding thruster. In AIAA/SAE/ASEE joint propulsion conference
23. Grimaud L et al (2016) Perturbations induced by electrostatic probe in the discharge of Hall thrusters. *Rev Sci Instrum* 87(4)
24. Jorns B, Goebel DM, Hofer RR (2015) Plasma perturbations in high-speed probing of hall thruster discharge chambers: quantification and mitigation. In 51st AIAA/SAE/ASEE joint propulsion conference
25. Wegner T et al (2021) Two-photon absorption laser induced fluorescence (TALIF) of neutral xenon in a hall effect thruster plasma. In AIAA propulsion & energy forum
26. Gottfried J et al (2023) Preliminary Krypton measurements by two-photon absorption laser induced fluorescence (TALIF) in cold flow and a Hollow Cathode Plasma. In AIAA SCITECH 2023 forum. American Institute of Aeronautics and Astronautics
27. Antozzi S et al (2023) Spatially resolved measurements of Krypton by two-photon absorption laser induced fluorescence (TALIF) in a Barium Oxide Hollow Cathode plasma. In AIAA Aviation 2023 Forum. American Institute of Aeronautics and Astronautics
28. Eichhorn C et al (2022) Single- and two-photon absorption laser-induced fluorescence spectroscopy in rare gases for gridded ion thruster diagnostics. *EPJ Techniques Instrum* 9(1):2
29. Eichhorn C et al (2019) Two-Photon Laser-induced fluorescence diagnostics of a radiofrequency ion thruster: measurements in Xenon and Krypton. In International electric propulsion conference. Vienna, Austria
30. Eichhorn C et al (2007) Multi-photon spectroscopy on Xenon for application on ion thruster plasma parameter investigations: experiment and theory. In IEPC. Florence, Italy: EPRS
31. Crofton MW et al (2013) Neutral Xenon density in the SPT-140 near-field plume. In International electric propulsion conference. Washington, D.C
32. Crofton M (1996) Measurement of neutral xenon density profile in an ion thruster plume. In 27th plasma dynamics and lasers conference. American Institute of Aeronautics and Astronautics
33. Tsukizaki R et al (2019) Neutral density measurement of microwave cathode by two-photon absorption LIF. In 36th International electric propulsion conference. Vienna, Austria
34. Gottfried J et al (2024) Temporally resolved neutral density measurements of Hall effect thruster breathing mode by two-photon absorption laser induced fluorescence (TALIF). In AIAA Scitech 2024 Forum. American Institute of Aeronautics and Astronautics
35. Dale ET, Jorns B (2019) Frequency scaling of the hall thruster breathing mode. In AIAA propulsion and energy 2019 forum. American Institute of Aeronautics and Astronautics
36. Hara K (2019) An overview of discharge plasma modeling for Hall effect thrusters. *Plasma Sources Sci Technol* 28(4):044001
37. Mullins CR et al (2017) Non-invasive hall current distribution measurement in a hall effect thruster. *Rev Sci Instrum* 88(1)
38. Wegner T, Dumitrache C, Yalin AP (2022) Rate-equation modeling of Xe and Kr TALIF for electric propulsion applications. In 37th International electric propulsion conference. Cambridge, MA, USA

Publisher's Note

Springer Nature remains neutral with regard to jurisdictional claims in published maps and institutional affiliations.